ACS APPLIED MATERIALS & INTERFACES

Research Article

www.acsami.org

Robust, Responsive, and Targeted PLGA Anticancer Nanomedicines by Combination of Reductively Cleavable Surfactant and Covalent Hyaluronic Acid Coating

Jintian Wu, Jian Zhang, Chao Deng,* Fenghua Meng, Ru Cheng, and Zhiyuan Zhong*

Biomedical Polymers Laboratory, College of Chemistry, Chemical Engineering and Materials Science, Soochow University, Suzhou 215123, People's Republic of China

Supporting Information

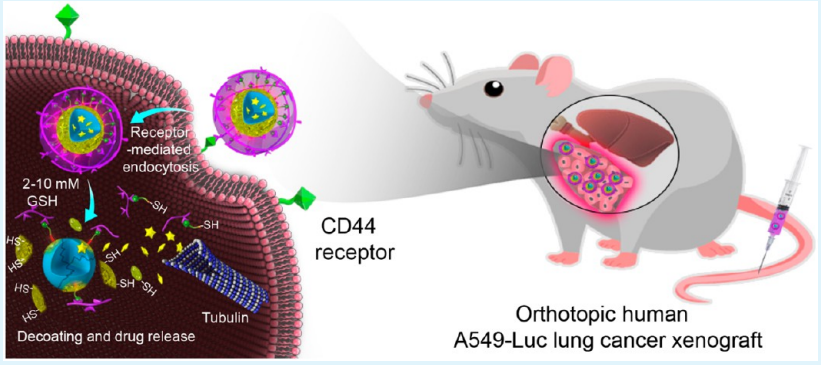

ABSTRACT: PLGA-based nanomedicines have enormous potential for targeted cancer therapy. To boost their stability, targetability, and intracellular drug release, here we developed novel multifunctional PLGA anticancer nanomedicines by combining a reductively cleavable surfactant (RCS), vitamin E−SS−oligo(methyl diglycol L-glutamate), with covalent hyaluronic acid (HA) coating. Reduction-sensitive HA-coated PLGA nanoparticles (rHPNPs) were obtained with small sizes of 55−61 nm and ζ potentials of −26.7 to −28.8 mV at 18.4−40.3 wt % RSC. rHPNPs were stable against dilution and 10% FBS while destabilized under reductive condition. The release studies revealed significantly accelerated docetaxel (DTX) release in the presence of 10 mM glutathione. DTX−rHPNPs exhibited potent and specific antitumor effect to CD44 + A549 lung cancer cells (IC_{50} = 0.52 μg DTX equiv/mL). The in vivo studies demonstrated that DTX−rHPNPs had an extended circulation time and greatly enhanced tolerance in mice. Strikingly, DTX−rHPNPs completely inhibited growth of orthotopic human A549-Luc lung tumor in mice, leading to a significantly improved survival rate and reduced adverse effect as compared to free DTX. This study highlights that advanced nanomedicines can be rationally designed by combining functional surfactants and surface coating.

KEYWORDS: *reduction-responsive, surfactant, PLGA nanoparticles, surface coating, docetaxel, lung cancer*

1. INTRODUCTION

PLGA nanoparticles are one of the most attractive pharmaceutical delivery nanoplatforms.[1−5] PLGA-based nanomedicines (e.g., Lupron Depot, Decapeptyl, and BIND-014) have been developed for treating different cancers including prostate and lung cancers.[6−9] In recent years, great endeavors have been devoted to improving PLGA-based nanomedicines.[10−12] For example, to improve their stability, PLGA-based nanomedicines were coated with *N*-trimethyl chitosan chloride via electrostatic interaction[13] or photo-cross-linked using poly(propylene fumarate)−*co*-PLGA.[14] To improve their cancer specificity, different targeting ligands such as *S*,*S*-2-(3-(5-amino-1-carboxypentyl)-ureido)-pentanedioic acid,[8,15] CXCR4,[16] folate, and cell-penetrating peptide R_7[17] have been used to decorate PLGA nanomedicines. To enhance their drug release in target site, pH-responsive PLGA nanoparticles have been developed by loading ammonium bicarbonate, which could be decomposed to NH_3 and CO_2 at endo- and lysomal pH[18] or incorporating pH sensitive poly(β-amino ester).[19] Reduction-sensitive PLGA nanoparticles were prepared by coating with PEG−SS−hexadecyl.[20] Dual-responsive PLGA nanoparticles were developed from PEG−PLGA−poly(L-glutamic acid) (PEG−PLGA−PGlu) that exhibited rapid response to both endosomal pH and proteinase K.[21] It should be noted that most of these advanced PLGA nanomedicines are designed to solve one or two delivery issues. We recently found that PLGA nanoparticles obtained via nanoprecipitation using vitamin E-oligo(methyl diglycol L-glutamate) (VEOEG) as a surfactant followed by covalent hyaluronic acid (HA) coating had high stability and targetability to MCF-7 breast and A549 lung tumors in vivo.[22,23]

Received: November 24, 2016
Accepted: January 12, 2017
Published: January 12, 2017

DOI: 10.1021/acsami.6b15105
ACS Appl. Mater. Interfaces 2017, 9, 3985−3994

These HA-coated nanoparticles, however, displayed a relatively large size of ∼150 nm as well as slow and incomplete release of paclitaxel and docetaxel (DTX) in 7 days. The size of nanotherapeutics is reported to play a critical role in tumor penetration and treatment efficacy in vivo.[24,25] Nanotherapeutics with smaller sizes (<100 nm) is generally more desirable.[26−28] The slow drug release would greatly reduce drug efficacy and possibly induce drug resistance.[29,30] Hence, it would be of great interest to fabricate small-sized HA-coated PLGA anticancer nanomedicines with a rapidly responsive drug release property.

Here, we describe development of robust, bioresponsive, and targeted PLGA anticancer nanomedicines by combining a reductively cleavable surfactant (RCS), vitamin E−SS−oligo-(methyl diglycol L-glutamate) (VE−SS−OEG), with HA coating (Scheme 1). VE−SS−OEG provides not only amino groups on nanoparticle surface to facilitate HA coating but also redox sensitivity to facilitate decoating and drug release within cancer cells. The engineering of sheddable shells and coatings has shown to be an effective way to realize fast intracellular drug release and improved antitumor performances in vitro and in vivo.[31−36] HA on surface of nanoparticles has been reported to facilitate cellular uptake of nanotherapeutics in CD44-overexpressing cancer cells.[37−39] HA coating affords not only high stability and minimum drug leakage but also high specificity toward CD44-positive cells.[40−43] Notably, our results show that DTX-loaded reduction-sensitive HA-coated PLGA nanoparticles (DTX−rHPNPs) are robust, small (55−61 nm), selective to human A549-Luc lung cancer cells, and capable of quickly releasing DTX in response to cytoplasmic reductive conditions, leading to complete inhibition of tumor growth and significantly improved survival of orthotopic human A549-Luc lung tumor-bearing nude mice. This is a first proof-of-concept study on design and fabrication of robust, bioresponsive, and small-sized PLGA nanomedicines using reductively cleavable surfactant for targeted tumor therapy.

2. EXPERIMENTAL SECTION

2.1. Preparation of Vitamin E−Disulfide−Oligo(Methyl Diglycol L-Glutamate). Vitamin E−disulfide−oligo(methyl diglycol L-glutamate (VE−SS−OEG) was prepared by polymerization of EG_2−Glu−NCA in the presence of VE cystamine conjugate (VE−SS−NH_2). Under N_2 atmosphere, DCM solution (38 mL) of VE-SS-NH_2 (1.19 g, 1.96 mmol) was added to a solution of EG_2−Glu−NCA (3.78 g, 13.73 mmol) in DCM (38 mL). After 12 h stirring at 25 °C, the reaction mixture was condensed by rotary evaporator, and precipitated in diethyl ether. VE−SS−OEG was dried in vacuo. Yield: 67.8%. ^{1}H nuclear magnetic resonance (^{1}H NMR) (600 MHz, $CDCl_3$, Figure 1, δ): 4.25−3.94 (−NHCOC**H**−, $CH_3OCH_2CH_2OCH_2C\mathbf{H_2}$−); 3.68−3.52 ($CH_3OC\mathbf{H_2}C\mathbf{H_2}OCH_2CH_2$−); 3.40−3.33 (−$C\mathbf{H_2}CH_2SSCH_2C\mathbf{H_2}$−, $\mathbf{CH_3}OCH_2CH_2OCH_2CH_2$−); 2.92 (−$C\mathbf{H_2}SSC\mathbf{H_2}$−); 2.71−2.53 (−$Ph(CH_3)_3C\mathbf{H_2}CH_2$−, −$COCH(NH)CH_2C\mathbf{H_2}$−); 2.25−1.75 (−$Ph(C\mathbf{H_3})_3$−, −$COCH(NH)C\mathbf{H_2}CH_2$−, −$Ph(CH_3)_3CH_2C\mathbf{H_2}$−); 1.54 ($CH_3(C\mathbf{H}(CH_3)CH_2CH_2CH_2)_3$−); 1.38−1.05 ($CH_3(CH(CH_3)C\mathbf{H_2}C\mathbf{H_2}C\mathbf{H_2})_3$−, −$C(C\mathbf{H_3})(CH_2)$−); 0.87−0.83 ($C\mathbf{H_3}(CH(C\mathbf{H_3})CH_2CH_2CH_2)_3$−). The ^{1}H NMR showed that VE-SS-OEG had a degree of polymerization of 6.3 (VE−SS−$OEG_{6.3}$). The structure of VE−SS−OEG was also confirmed by matrix-assisted laser desorption−ionization time-of-flight (MALDI-TOF) analysis, and the terminal amino functionality was quantified by 2,4,6-trinitrobenzenesulfonic

Scheme 1. Illustration of Reduction-Sensitive HA-Coated PLGA Nanoparticles for Targeted DTX Delivery to Orthotopic Human A549-Luc Lung Xenografts

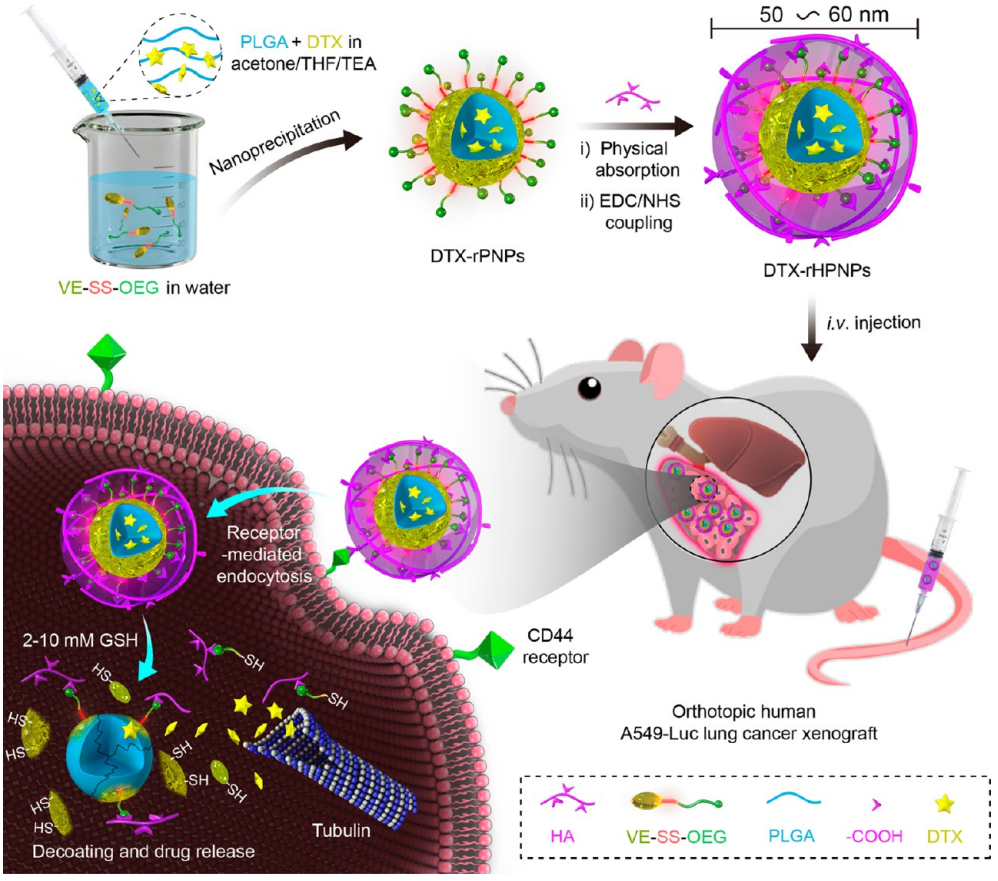

DOI: 10.1021/acsami.6b15105
ACS Appl. Mater. Interfaces 2017, 9, 3985−3994

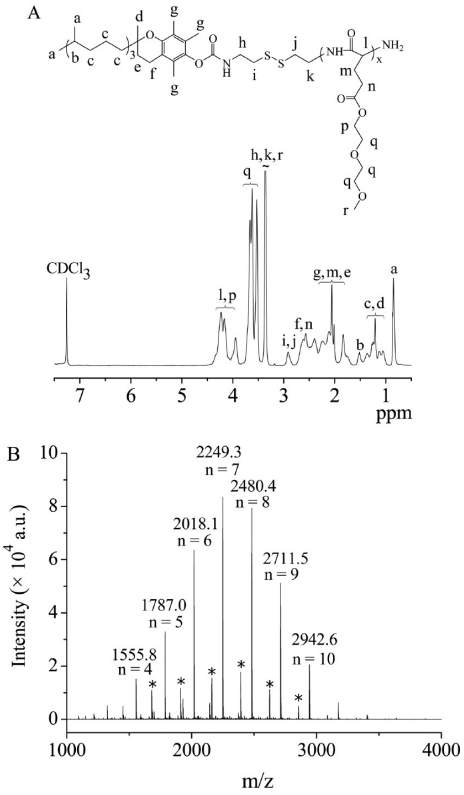

Figure 1. Characterization of VE−SS−$OEG_{6.3}$. (A) ^1H NMR spectrum (600 MHz, $CDCl_3$), and (B) MALDI-TOF mass spectrum. $m/z = M_n + Na^+ = 608.4 + 231.1 \times n + 23.0$, wherein n denotes the number of repeating units of EG_2−Glu, and * indicates backbiting byproducts.

acid (TNBSA) assay. VE-SS-OEG could self-assemble into micelles in water. The critical micelle concentration of VE-SS-OEG was determined using pyrene as a fluorescent probe.[22]

2.2. Preparation of Redox-Sensitive Hyaluronic Acid Coated PLGA Nanoparticles. Reduction-sensitive PLGA nanoparticles (rPNPs) were prepared using VE−SS−OEG as a reductively cleavable surfactant (RCS) by a modified nanoprecipitation method.[44] Briefly, PLGA was dissolved in a mixed solution of acetone, tetrahydrofuran, and triethylamine (v/v/v, 40:6:1) to obtain a PLGA solution (10.0 mg/mL). A total of 705 μL of the above solution was quickly added to 9.0 mL of aqueous solution of VE−SS−OEG (18.4, 31.0, or 40.3 wt % of VE−SS−OEG and PLGA total weight) under stirring at 37 °C. After stirring for 6 h at room temperature, the residual organic solvent was removed by evaporation. The aqueous phase was extensively dialyzed against deionized water and lyophilized to obtain rPNPs. rHPNPs were prepared through coating rPNPs with negatively charged HA followed by covalent cross-linking reaction between amino groups on the surface of rPNPs and carboxyl groups of HA, as previously reported.[22] The stability of rHPNPs against 1000-fold dilution and 10% fetal bovine serum (FBS), as well as their responsivity to 10 mM glutathione, was monitored by DLS. To monitor their intracellular trafficking and in vivo tumor-targetability, near-infrared fluorescence probe Cy5 grafted HA[22] was used to coat rPNPs yielding Cy5-labeled rHPNPs (Cy5−rHPNPs).

2.3. MTT Assays. The cytotoxicity of bare nanoparticles was studied by MTT assays. A549-Luciferase (A549-Luc) human lung cancer cells and L929 mouse fibroblast cells were cultured in 96 well plates (8.0×10^3 cells per well) for 24 h and then incubated with prescribed amounts of rHPNPs (10, 50, 150, 300, and 600 μg/mL) at 37 °C in 5% CO_2 atmosphere for 48 h. The cells following the addition of MTT solution in PBS (10 μL, 5 mg/mL) were incubated for 4 h at 37 °C. After careful removal of the supernatant, the MTT−formazan generated by live cells was dissolved in DMSO (150 μL), and the absorbance at a wavelength of 492 nm was measured using a microplate reader (Multiskan FC, Thermo Scientific). The cell viability (%) was determined by comparing the absorbance with control wells containing only cell-culture medium.

The antitumor activity of DTX-rHPNPs was evaluated in a similar way except that the cells were incubated with DTX−rHPNPs for 4 h and then cultured in a refreshed medium for another 44 h. Free DTX dissolved in Tween 80 and ethanol (v/v = 1:1) was used as a control. The inhibition experiment was performed by pretreating A549-Luc cells with free HA (5 mg/mL) for 4 h prior to incubating with DTX−rHPNPs. The IC_{50} of DTX−rHPNPs was calculated by curve fitting of the cell viability versus drug concentrations (n = 4).

2.4. In Vivo Antitumor Efficacy of DTX−rHPNPs. The in vivo antitumor efficacy of DTX−rHPNPs was investigated using the nude mice bearing orthotopic human A549-Luc lung cancer xenografts. All mice studies were performed under protocols approved by the Animal Care and Use Committee of Soochow University. Orthotopic lung cancer model was built by directly injecting 5×10^6 A549-Luc cells suspended in 50 μL of matrigel/PB (1/4, v/v) into the left lung parenchyma of mice.[45,46] The tumor size and sites were monitored by the measuring bioluminescence through IVIS Lumina II imaging system (Caliper Life Sciences) after the intravenous injection of D-luciferin potassium salt solution (15 mg/mL, 100 μL) in PBS. Treatments were started when luminescence intensity of lung tumor reached about 1×10^6 p/s/cm^2/sr, and this day was designated as day 0. The mice were randomly divided (six mice per group) and treated via the intravenous injection of DTX−rHPNPs or free DTX at a DTX dosage of 5 mg/kg on day 0, 4, 8, and 12, respectively. A single-dose treatment was also evaluated by the administration of DTX−rHPNPs formulation at 15 mg DTX/kg in 0.15 mL of PBS on day 0. Bare rHPNPs and PBS were used as controls. The treatment effect was assessed by measuring the luminescence intensity of lung tumor. Mice were weighed and normalized to their initial weights. Mice with the weight loss of over 15% were considered to be dead during treatment.

Scheme 2. Synthesis of VE−SS−OEG[a]

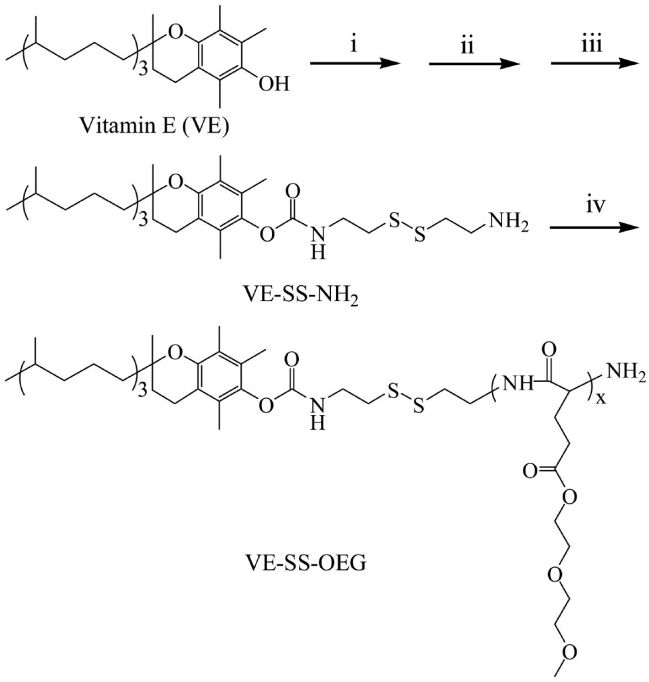

[a]Conditions: (i) 4-nitrophenyl chloroformate, pyridine, 30 °C, 24 h; (ii) NH_2−Cys−Boc, pyridine, 30 °C, 24 h; (iii) CF_3COOH−HCl, 0 °C, 6 h; (iv) EG_2−Glu−NCA, 25 °C, 12 h.

3. RESULTS AND DISCUSSION

3.1. Synthesis of VE−SS−OEG. VE−SS−OEG was readily acquired by polymerization of EG_2−Glu−NCA using VE−SS−NH_2

DOI: 10.1021/acsami.6b15105
ACS Appl. Mater. Interfaces 2017, 9, 3985−3994

as an initiator that was prepared through coupling NH_2−Cys−Boc to vitamin E followed by the deprotection of Boc (Scheme 2). ^{1}H NMR of VE−SS−NH_2 showed besides characteristic signals of VE also signals assignable to cystamine moieties (δ: 2.79, 2.88, 3.03, and 3.61) (Figure S1). The methylene protons at δ 2.58 (vitamin E) and 3.03 (cystamine) had equal integrals, corroborating successful coupling of vitamin E and cystamine. The ROP of EG_2−Glu−NCA was carried out in DCM at 25 °C. ^{1}H NMR of VE−SS−OEG detected signals attributed to the OEG block (δ 4.25−3.94, 3.68−3.52, 3.40−3.33, and 2.71−2.53) and vitamin E group (δ 2.25−1.75, 1.54, 1.38−1.05, and 0.87−0.83) (Figure 1A). Interestingly, VE−SS−OEG had degree of polymerization (DP) of 6.3−12.2, calculated by comparing the intensities of signals at δ 3.68−3.52 and δ 0.87−0.83, close to the monomer-to-initiator molar ratios (Table 1). VE−SS−OEG had low polydispersities of 1.12−1.24 as characterized by GPC measurements (Table 1). MALDI-TOF analysis of VE-SS-$OEG_{6.3}$ confirmed its low polydispersity and well-controlled molecular weight (Figure 1B). Notably, a minor mass distribution with cyclic pyroglutamate end group instead of amino end group was observed, which is due to occurrence of backbiting reaction.[22,47] TNBSA analysis revealed that 63.2% VE−SS−OEG had an amino end group. VE−SS−OEG possessed a HLB value of 14.1−16.4 and could self-assemble into micelles in aqueous medium with a CMC of 190−199 mg/L (Table 1).

Table 1. Characteristics of VE−SS−OEG

			M_n (kg/mol)				
entry	$[M]_0/[I]_0$	DP ^{1}H NMR[a]	^{1}H NMR[a]	GPC[b]	Đ GPC[b]	CMC[c] (mg/L)	HLB[d]
1	7	6.3	2.1	1.9	1.12	190.8	14.1
2	10	9.6	2.8	2.1	1.19	192.4	15.7
3	13	12.2	3.4	2.9	1.24	198.9	16.4

[a]Calculated from ^{1}H NMR. [b]Determined by GPC (standard: poly(methyl methacrylate)). [c]Determined using pyrene as a fluorescence probe. [d]$(HLB)_G = 20 \times M_H/(M_H + M_L)$, in which M_H and M_L are the molecular weight of hydrophobic and hydrophilic chain, respectively.

3.2. Preparation and Characterization of rPNPs and rHPNPs. PLGA nanoparticles were fabricated via nanoprecipitation method using VE−SS−OEG as a surfactant. As revealed by DLS, rPNPs prepared at 18.4−40.3 wt % VE−SS−OEG had small sizes (~55 nm) and low polydispersity indices (PDI) (Figure 2A and Table 2). Figure 2B reveals that rPNPs were spherical and had a small size similar to that determined from DLS. Notably, rPNPs formed with VE−SS−OEG could maintain their structures during centrifugation and over 1 week storage. Taking advantages of amino groups on the nanoparticle surface, various biomolecules could be easily decorated on nanoparticles to form multifunctional PLGA nanoparticles. Here, HA was coated on nanoparticles via physical absorption and 1-ethyl-3-(3-dimethylaminopropyl)-carbodiimide hydrochloride−*N*-hydroxysuccinimide (EDC−NHS) coupling reaction, yielding tumor-targeting rHPNPs. DLS and TEM showed that rHPNPs retained small sizes and narrow PDI (Figure 2A,B). rHPNPs were about 3−6 nm bigger than rPNPs (Table 2). In comparison, PLGA nanoparticles prepared using reduction-insensitive VEOEG surfactant had a much larger size (~150 nm).[22,23] ζ potential measurements revealed that coating of rPNPs with HA resulted in 7.5−12.8 mV more negative surface charge. The larger particle size and higher negative surface charge of rHPNPs than rPNPs supports coating of rPNPs with HA. Using Cy5-labeled HA as a model, HA content was shown to increase from 6.5 to 13.1 wt % with

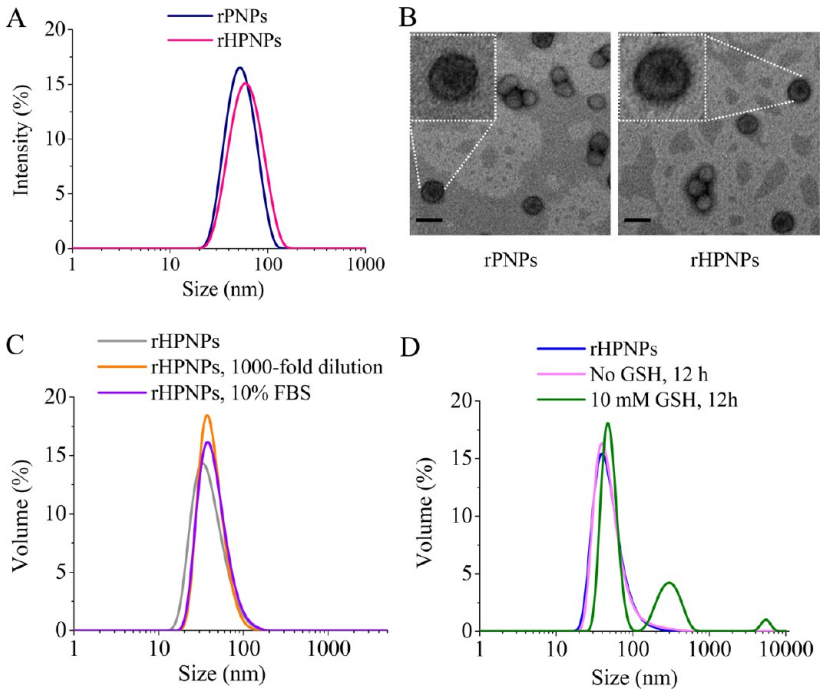

Figure 2. Characteristics of rPNPs and rHPNPs formed at 40.3 wt % VE−SS−OEG. (A) Size distribution of rPNPs and rHPNPs determined by DLS; (B) TEM images of rPNPs and rHPNPs (dropping 15 μL of 0.25 mg/mL nanoparticle suspension on the copper grid followed by staining with 1 wt % phosphotungstic acid, scale bar: 50 nm); (C) stability of rHPNPs against extensive dilution and 10% FBS; (D) change of rHPNPs size and distribution in response to 10 mM GSH at 37 °C determined by DLS.

DOI: 10.1021/acsami.6b15105
ACS Appl. Mater. Interfaces 2017, 9, 3985−3994

Table 2. Characteristics of rPNPs and rHPNPs

	rPNPs				rHPNPs			
entry	VE−SS−OEG content (wt %)	size[a] (nm)	PDI[a]	ζ[b] (mV)	size[a] (nm)	PDI[a]	ζ[b] (mV)	HA content[c] (wt %)
1	18.4	55	0.14	−19.2	61	0.15	−26.7	6.5
2	31.0	54	0.13	−16.9	59	0.15	−28.4	10.3
3	40.3	52	0.10	−16.0	55	0.13	−28.8	13.1

[a]Determined by DLS using a Zetasizer Nano-ZS. [b]Measured using a Zetasizer Nano-ZS equipped with a standard capillary electrophoresis cell. [c]Determined by fluorescence measurements at 662 nm using Cy5 as a fluorescence probe.

increasing VE−SS−OEG content from 18.4 to 40.3 wt % (Table 2). To acquire high-stability and abundant HA for tumor-targetability, rHPNPs with 13.1 wt % of HA were selected for the following experiments. As expected, cross-linked rHPNPs exhibited negligible size change against 1000-fold dilution and in 10% FBS for 12 h (Figure 2C), suggesting they have high colloidal stability. Cross-linked nanotherapeutics has been extensively explored to avoid premature drug release during circulation and enhance targeting delivery of drugs in tumor sites.[48,49] Under the condition of 10 mM GSH, rHPNPs swelled and aggregated in 12 h (Figure 2D), demonstrating that rHPNPs are redox-sensitive. We and others have shown that micelles following shedding off shells and nanoparticles following decoating are prone to aggregation.[50,51] Thus, rHPNPs have remarkable stability but tend to decoat the HA layer inside cells.

3.3. DTX Loading and Release. DTX was loaded into rHPNPs at a theoretical drug loading content (DLC) of 10 or 20 wt %. Notably, DTX-loaded rHPNPs exhibited a small size of 56−58 nm and a low PDI of 0.11−0.12. The ζ potential measurements showed that DTX−rHPNPs had negative surface charge of ca. −30 mV (Table 3), supporting the fact

Table 3. Characteristics of DTX−rPNPs and DTX−rHPNPs prepared at 40.3 wt % VE−SS−OEG

		DTX−rPNPs		DTX−rHPNPs				
entry	DLC theory (wt %)	size[a] (nm)	PDI[a]	size[a] (nm)	PDI[a]	ζ[b] (mV)	DLC[c] (wt %)	DLE[c] (%)
1	10	53	0.13	56	0.12	−30.0	6.5	63.8
2	20	54	0.12	58	0.11	−29.4	11.2	51.5

[a]Determined by DLS using Zetasizer Nano-ZS. [b]Measured using Zetasizer Nano-ZS equipped with a standard capillary electrophoresis cell. [c]Determined by HPLC.

that nanoparticles were coated with negatively charged HA that has been extensively reported to have excellent tumor-targetability toward CD44+ cancer cells.[52−57] DTX−rHPNPs showed a decent DLC of 11.2 wt % at a theoretical DLC of 20 wt %. Interestingly, DTX−rHPNPs could be freeze-dried and redispersed in PB buffer, which would largely facilitate their storage, scale-up fabrication, and clinic applications.[52,58] In the following, DTX−rHPNPs with a DLC of 11.2 wt % was selected for in vitro drug release and cell and animal experiments. DTX−rHPNPs exhibited high stability and slow DTX release under physiological conditions in which less than 30% of DTX was released in 48 h (Figure 3). In contrast, nearly 80% of DTX was released with addition of 10 mM GSH. Hence, drug release from DTX−rHPNPs is triggered by GSH. Compared to free drugs, PLGA-based nanotherapeutics with intracellular triggered drug release have exhibited significantly enhanced antitumor efficacy on various solid tumors and drug-resistant tumors.[59,60]

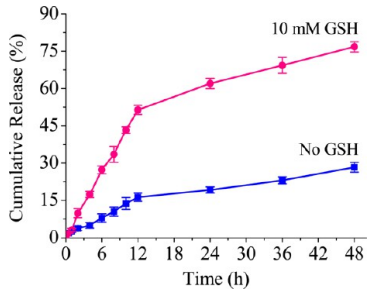

Figure 3. GSH-triggered drug release of DTX−rHPNPs (nanoparticle concentration: 0.2 mg/mL) at pH 7.4 and 37 °C in PB buffer (10 mM) (n = 3).

3.4. Targetability and Antitumor Activity of DTX−rHPNPs. For the study of their tumor targetability, rHPNPs were labeled with Cy5. Flow cytometry showed efficient uptake of Cy5-rHPNPs by CD44-overexpressing A549-Luc cells in 4 h (Figure 4A). Notably, the uptake of Cy5−rHPNPs was

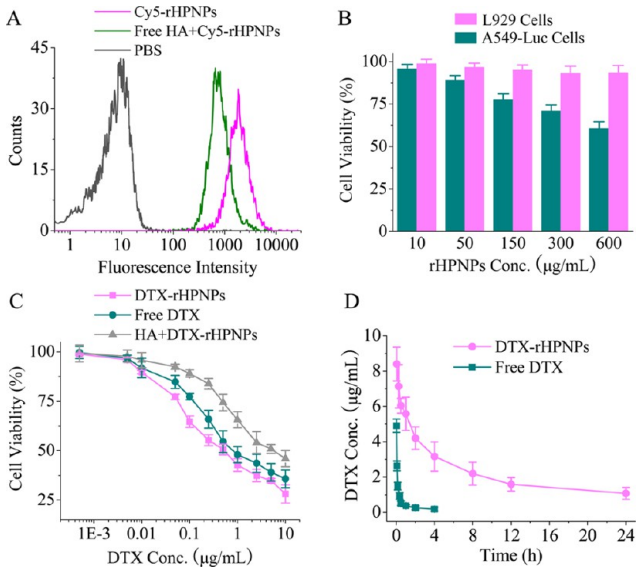

Figure 4. (A) Flow cytometry study. A549-Luc cells were incubated for 4 h with Cy5−rHPNPs (5.0 μg Cy5/mL); (B) cytotoxicity of bare rHPNPs in L929 and A549-Luc cells after 48 h of incubation; (C) antitumor activity of DTX−rHPNPs in A549-Luc cells (mean ± SD, n = 4); (D) in vivo pharmacokinetics of DTX−rHPNPs and free DTX in mice (means ± SD, n = 3).

significantly reduced by pretreating A549-Luc cells for 4 h with free HA, indicating that rHPNPs are internalized by A549-Luc cells via receptor-mediated internalization.

MTT assays indicated that bare rHPNPs appeared nontoxic to normal cells like L929 cells, while it exhibited moderate cytotoxicity toward A549-Luc lung cancer cells (Figure 4B).

DOI: 10.1021/acsami.6b15105
ACS Appl. Mater. Interfaces 2017, 9, 3985−3994

For example, L929 and A549-Luc cells following 48 h incubation with 600 μg/mL bare rHPNPs displayed cell viabilities of 93% and 61%, respectively. We and other groups found that VE conjugates and nanoparticles coated with VE−oligopeptide were toxic toward cancer cells.[22,61,62] Interestingly, DTX−rHPNPs exhibited a high inhibitory effect toward A549-Luc cells with IC_{50} = 0.52 μg DTX equiv/mL (rHPNPs concentration =4.12 μg/mL), which was even lower than that of free DTX (0.87 μg/mL) (Figure 4C). In comparison, reduction-insensitive DTX−HPNPs showed an IC_{50} of 0.91 μg DTX equiv/mL to A549-Luc cells.[23] The high antitumor effect of DTX−rHPNPs is likely due to their efficient internalization by A549-Luc cells, redox-triggered drug release, and presence of VE−SS−OEG. The antitumor activity of DTX−rHPNPs was, however, markedly truncated after treating A549-Luc cells by free HA (Figure 4C), in line with their excellent targetability to A549-Luc cells.

3.5. In Vivo Pharmacokinetics and Antitumor Efficacy of DTX−rHPNPs. HPLC quantification of DTX levels in the blood after intravenous injection of DTX−rHPNPs revealed that DTX−rHPNPs had an over 12-fold longer circulation time than free DTX (3.85 versus 0.32 h) (Figure 4D). The long plasma retention of DTX−rHPNPs is likely due to their superb colloidal stability, small size, and inhibited drug leakage.

DTX−rHPNPs was used to treat orthotopic human A549-Luc lung tumor-bearing mice. The mice, following the intravenous injection of DTX−rHPNPs (5 mg DTX/kg), exhibited weak bioluminescence over the whole treatment period of 16 days (Figure 5A), indicating that DTX−rHPNPs can completely suppress tumor growth. In contrast, mice treated with free DTX, bare rHPNPs, and PBS displayed incessant tumor growth. The semiquantitative analysis of radiance corroborated that DTX−rHPNPs caused significantly more effective tumor inhibition than free DTX, while bare rHPNPs had little antitumor effect (Figure 5B). The pictures of tumors excised on day 16 confirmed that DTX−rHPNPs group possessed negligible tumor luminescence and invasion in the lung, while tumor not only occupied the whole lung but also invaded into heart tissue in PBS group (Figure 5C). Encouraged by their excellent therapeutic efficacy, we further evaluated the antitumor effect of DTX−rHPNPs at a single dose (sd). Single-dosing scheme has attracted recent interests due to a better compliance with patients.[63,64] Interestingly, the results showed that a single dose of DTX-rHPNPs (15 mg DTX equiv/kg) led

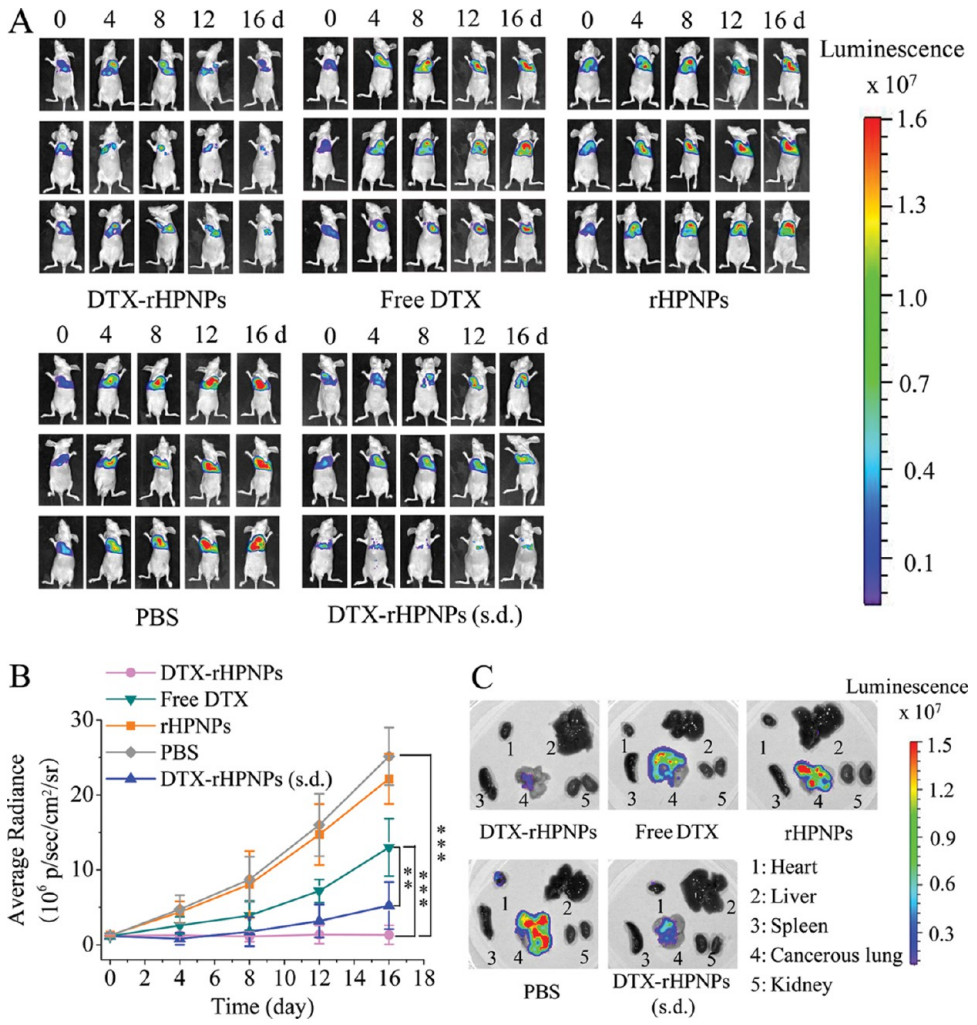

Figure 5. Orthotopic human A549-Luc lung tumor-bearing mice treated with DTX−rHPNPs, free DTX, rHPNPs, PBS, or DTX−rHPNPs (sd). (A) Luminescence optical imaging of cancerous lung; (B) quantified average luminescence levels of cancerous lung. The in vivo luminescent images were normalized and reported as photons/s/cm^2/sr; and (C) ex vivo imaging of major organs and cancerous lung collected from different treatment groups on day 16. Double asterisks indicate $p < 0.01$, and triple asterisks indicate $p < 0.001$ (Student's t test, $n = 6$).

DOI: 10.1021/acsami.6b15105
ACS Appl. Mater. Interfaces 2017, 9, 3985−3994

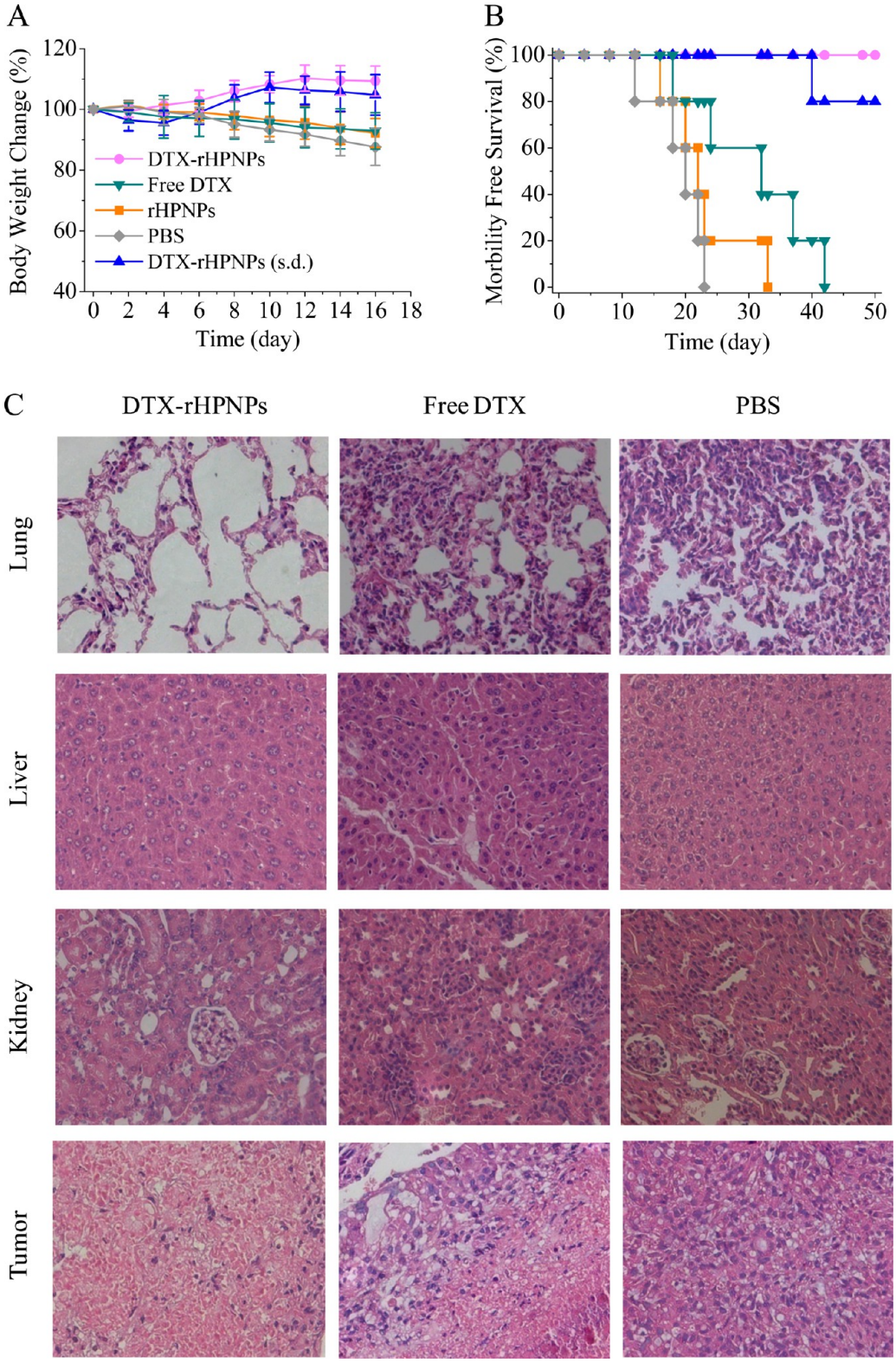

Figure 6. Body weight changes (n = 6) (A), survival rates (n = 5) (B), and histological analysis (C) after 16 days of treatment of orthotopic human A549-Luc lung tumor-bearing nude mice. The images were obtained at high magnification (400×).

to significantly more effective inhibition of tumor growth than multiple injection of free DTX (Figure 5B).

Owing to tumor invasion, mice treated with bare rHPNPs and PBS exhibited gradual body weight loss (about 7.9% and 12.4%, respectively, at day 16) (Figure 6A). On the contrary, increased body weight was observed for mice treated with DTX−rHPNPs, corroborating that DTX−rHPNPs effectively suppress tumor invasion and cause little adverse effects. Notably, mice treated with a single dose of DTX−rHPNPs showed also increased body weight after initial slight loss of body weight. Consistently, DTX−rHPNPs remarkably increased the survival rates of A549-Luc lung-tumor-bearing mice (Figure 6B). All mice

DOI: 10.1021/acsami.6b15105
ACS Appl. Mater. Interfaces 2017, 9, 3985−3994

treated with multiple doses of DTX−rHPNPs survived over an experimental period of 50 days. Even single dosing of DTX−rHPNPs led to 80% mice survival in 50 days. In contrast, short median survival times of 20 and 22 days were observed for PBS and bare rHPNPs groups, respectively. The mice treated with PBS and bare rHPNPs showed shortness of breath, sluggish, and loss of appetite over time due to fast tumor invasion. Free DTX group exhibited a moderate median survival time of 32 days. The histological analyses using hematoxylin and eosin staining revealed extensive nuclei lysis of tumor tissue in both DTX−rHPNPs and free DTX groups (Figure 6C). Moreover, unlike free DTX-treated mice, DTX−rHPNPs groups exhibited well-organized lung tissue and little liver and kidney damage. As expected, pronounced lung damage including disrupted alveolar structure was observed in mice treated with rHPNPs or PBS (Figure S2), causing respiratory failure and eventually death. It is evident that DTX−rHPNPs achieve efficacious and selective delivery of DTX to CD44 positive orthotopic human A549-Luc lung tumor xenografts, leading to efficient tumor inhibition, reduced systemic side effects, and markedly improved survival rates.

4. CONCLUSIONS

We have demonstrated that robust, bioresponsive, and targeted PLGA anticancer nanomedicines can be conveniently developed by combining a reductively cleavable surfactant with hyaluronic acid coating. The in vitro and in vivo results show that docetaxel-loaded redox-sensitive HA-coated PLGA nanoparticles (DTX−rHPNPs) possess superior stability, potent antitumor activity, long circulation time, high targetability, and effective inhibition of orthotopic human A549-Luc lung tumor in nude mice. In accordance, DTX−rHPNPs lead to superior survival rate and significantly reduced adverse effects in orthotopic human A549-Luc lung tumor-bearing mice as compared to free DTX. To the best of our knowledge, this represents the first development of multifunctional PLGA-based anticancer nanomedicines by combining a reductively cleavable surfactant with hyaluronic acid coating. Notably, different lipophilic drugs can be loaded into rHPNPs to suit for different indications. The easy fabrication and multifunctional feature of rHPNPs render them a highly promising targeted nanoplatform for the effective treatment of various malignancies.

■ ASSOCIATED CONTENT

Supporting Information

The Supporting Information is available free of charge on the ACS Publications website at DOI: 10.1021/acsami.6b15105.

Additional details on materials, characterization, synthesis of VE-SS-NH_2, drug loading, in vitro drug release, flow cytometry analysis, pharmacokinetics studies, and histological analysis; figures showing the ^1H NMR spectrum for VE-SS-NH_2; and histological analysis of tumor and organs following the treatment with rHPNPs and DTX−rHPNPs. (PDF)

■ AUTHOR INFORMATION

Corresponding Authors

*E-mail: cdeng@suda.edu.cn. Tel: +86-512-65880098.
*E-mail: zyzhong@suda.edu.cn.

ORCID

Fenghua Meng: 0000-0002-8608-7738
Zhiyuan Zhong: 0000-0003-4175-4741

Notes

The authors declare no competing financial interest.

■ ACKNOWLEDGMENTS

This work was supported by the National Natural Science Foundation of China (NSFC grant nos. 51273137, 51473110, 51403147, and 51225302) and the Natural Science Foundation of Jiangsu Province (grant no. 14KJB150022).

■ REFERENCES

(1) Hu, C.-M. J.; Fang, R. H.; Wang, K.-C.; Luk, B. T.; Thamphiwatana, S.; Dehaini, D.; Nguyen, P.; Angsantikul, P.; Wen, C. H.; Kroll, A. V.; Carpenter, C.; Ramesh, M.; Qu, V.; Patel, S. H.; Zhu, J.; Shi, W.; Hofman, F. M.; Chen, T. C.; Gao, W.; Zhang, K.; et al. Nanoparticle Biointerfacing by Platelet Membrane Cloaking. *Nature* **2015**, *526*, 118−121.

(2) Danhier, F.; Ansorena, E.; Silva, J. M.; Coco, R.; Le Breton, A.; Preat, V. PLGA-Based Nanoparticles: An Overview of Biomedical Applications. *J. Controlled Release* **2012**, *161*, 505−522.

(3) Fredenberg, S.; Wahlgren, M.; Reslow, M.; Axelsson, A. The Mechanisms of Drug Release in Poly(Lactic-Co-Glycolic Acid)-Based Drug Delivery Systems-a Review. *Int. J. Pharm.* **2011**, *415*, 34−52.

(4) Ma, G. H. Microencapsulation of Protein Drugs for Drug Delivery: Strategy, Preparation, and Applications. *J. Controlled Release* **2014**, *193*, 324−340.

(5) Kumari, A.; Yadav, S. K.; Yadav, S. C. Biodegradable Polymeric Nanoparticles Based Drug Delivery Systems. *Colloids Surf., B* **2010**, *75*, 1−18.

(6) Mundargi, R. C.; Babu, V. R.; Rangaswamy, V.; Patel, P.; Aminabhavi, T. M. Nano/Micro Technologies for Delivering Macromolecular Therapeutics Using Poly(D,L-Lactide-Co-Glycolide) and Its Derivatives. *J. Controlled Release* **2008**, *125*, 193−209.

(7) Vermonden, T.; Censi, R.; Hennink, W. E. Hydrogels for Protein Delivery. *Chem. Rev.* **2012**, *112*, 2853−2888.

(8) Hrkach, J.; Von Hoff, D.; Ali, M. M.; Andrianova, E.; Auer, J.; Campbell, T.; De Witt, D.; Figa, M.; Figueiredo, M.; Horhota, A.; Low, S.; McDonnell, K.; Peeke, E.; Retnarajan, B.; Sabnis, A.; Schnipper, E.; Song, J. J.; Song, Y. H.; Summa, J.; Tompsett, D.; et al. Preclinical Development and Clinical Translation of a PSMA-Targeted Docetaxel Nanoparticle with a Differentiated Pharmacological Profile. *Sci. Transl. Med.* **2012**, *4*, 128ra39.

(9) Von Hoff, D. D.; Mita, M. M.; Ramanathan, R. K.; Weiss, G. J.; Mita, A. C.; LoRusso, P. M.; Burris, H. A., III; Hart, L. L.; Low, S. C.; Parsons, D. M.; Zale, S. E.; Summa, J. M.; Youssoufian, H.; Sachdev, J. C. Phase I Study of PSMA-Targeted Docetaxel-Containing Nanoparticle Bind-014 in Patients with Advanced Solid Tumors. *Clin. Cancer Res.* **2016**, *22*, 3157−3163.

(10) Fredman, G.; Kamaly, N.; Spolitu, S.; Milton, J.; Ghorpade, D.; Chiasson, R.; Kuriakose, G.; Perretti, M.; Farokhzad, O.; Tabas, I. Targeted Nanoparticles Containing the Proresolving Peptide Ac2−26 Protect against Advanced Atherosclerosis in Hypercholesterolemic Mice. *Sci. Transl. Med.* **2015**, *7*, 275ra20.

(11) Zhu, H. J.; Chen, H. B.; Zeng, X. W.; Wang, Z. Y.; Zhang, X. D.; Wu, Y. P.; Gao, Y. F.; Zhang, J. X.; Liu, K. W.; Liu, R. Y.; Cai, L. T.; Mei, L.; Feng, S. S. Co-Delivery of Chemotherapeutic Drugs with Vitamin E TPGS by Porous PLGA Nanoparticles for Enhanced Chemotherapy against Multi-Drug Resistance. *Biomaterials* **2014**, *35*, 2391−2400.

(12) Sanchez-Gaytan, B. L.; Fay, F.; Lobatto, M. E.; Tang, J.; Ouimet, M.; Kim, Y.; van der Staay, S. E. M.; van Rijs, S. M.; Priem, B.; Zhang, L. F.; Fisher, E. A.; Moore, K. J.; Langer, R.; Fayad, Z. A.; Mulder, W. J. M. HDL-Mimetic PLGA Nanoparticle to Target Atherosclerosis Plaque Macrophages. *Bioconjugate Chem.* **2015**, *26*, 443−451.

(13) Sheng, J. Y.; Han, L. M.; Qin, J.; Ru, G.; Li, R. X.; Wu, L. H.; Cui, D. Q.; Yang, P.; He, Y. W.; Wang, J. X. N-Trimethyl Chitosan Chloride-Coated PLGA Nanoparticles Overcoming Multiple Barriers to Oral Insulin Absorption. *ACS Appl. Mater. Interfaces* **2015**, *7*, 15430−15441.

DOI: 10.1021/acsami.6b15105
ACS Appl. Mater. Interfaces 2017, 9, 3985−3994

(14) Liu, X. F.; Miller, A. L., II; Yaszemski, M. J.; Lu, L. C. Biodegradable and Crosslinkable PPF-PLGA-PEG Self-Assembled Nanoparticles Dual-Decorated with Folic Acid Ligands and Rhodamine B Fluorescent Probes for Targeted Cancer Imaging. *RSC Adv.* **2015**, *5*, 33275−33282.
(15) Von Hoff, D. D.; Mita, M. M.; Ramanathan, R. K.; Weiss, G. J.; Mita, A. C.; LoRusso, P. M.; Burris, H. A., III; Hart, L. L.; Low, S. C.; Parsons, D. M.; Zale, S. E.; Summa, J. M.; Youssoufian, H.; Sachdev, J. C. Phase I Study of PSMA-Targeted Docetaxel-Containing Nanoparticle Bind-014 in Patients with Advanced Solid Tumors. *Clin. Cancer Res.* **2016**, *22*, 3157−3163.
(16) Gao, D. Y.; Lin, T. T.; Sung, Y. C.; Liu, Y. C.; Chiang, W. H.; Chang, C. C.; Liu, J. Y.; Chen, Y. C. CXCR4-Targeted Lipid-Coated PLGA Nanoparticles Deliver Sorafenib and Overcome Acquired Drug Resistance in Liver Cancer. *Biomaterials* **2015**, *67*, 194−203.
(17) Wang, Y.; Dou, L. M.; He, H. J.; Zhang, Y.; Shen, Q. Multifunctional Nanoparticles as Nanocarrier for Vincristine Sulfate Delivery to Overcome Tumor Multidrug Resistance. *Mol. Pharmaceutics* **2014**, *11*, 885−894.
(18) Liu, Q.; Chen, X. M.; Jia, J. L.; Zhang, W. F.; Yang, T. Y.; Wang, L. Y.; Ma, G. H. pH-Responsive Poly(D,L-Lactic-Co-Glycolic Acid) Nanoparticles with Rapid Antigen Release Behavior Promote Immune Response. *ACS Nano* **2015**, *9*, 4925−4938.
(19) Zhang, C.; An, T.; Wang, D.; Wan, G. Y.; Zhang, M. M.; Wang, H. M.; Zhang, S. P.; Li, R. S.; Yang, X. Y.; Wang, Y. S. Stepwise pH-Responsive Nanoparticles Containing Charge-Reversible Pullulan-Based Shells and Poly(Beta-Amino Ester)/Poly(Lactic-Co-Glycolic Acid) Cores as Carriers of Anticancer Drugs for Combination Therapy on Hepatocellular Carcinoma. *J. Controlled Release* **2016**, *226*, 193−204.
(20) Wu, B.; Yu, P.; Cui, C.; Wu, M.; Zhang, Y.; Liu, L.; Wang, C. X.; Zhuo, R. X.; Huang, S. W. Folate-Containing Reduction-Sensitive Lipid-Polymer Hybrid Nanoparticles for Targeted Delivery of Doxorubicin. *Biomater. Sci.* **2015**, *3*, 655−664.
(21) Xu, H. L.; Yang, D.; Cai, C. F.; Gou, J. X.; Zhang, Y.; Wang, L. H.; Zhong, H. J.; Tang, X. Dual-Responsive mPEG-PLGA-PGlu Hybrid-Core Nanoparticles with a High Drug Loading to Reverse the Multidrug Resistance of Breast Cancer: An in Vitro and in Vivo Evaluation. *Acta Biomater.* **2015**, *16*, 156−168.
(22) Wu, J.; Zhang, J.; Deng, C.; Meng, F.; Zhong, Z. Vitamin E-Oligo (Methyl Diglycol L-Glutamate) as a Biocompatible and Functional Surfactant for Facile Preparation of Active Tumor-Targeting PLGA Nanoparticles. *Biomacromolecules* **2016**, *17*, 2367−2374.
(23) Wu, J.; Deng, C.; Meng, F.; Zhang, J.; Sun, H.; Zhong, Z. Hyaluronic Acid Coated PLGA Nanoparticles Docetaxel Effectively Targets and Suppresses Orthotopic Human Lung Cancer. *J. Controlled Release* **2016**, DOI: 10.1016/j.jconrel.2016.12.024.
(24) Petros, R. A.; DeSimone, J. M. Strategies in the Design of Nanoparticles for Therapeutic Applications. *Nat. Rev. Drug Discovery* **2010**, *9*, 615−627.
(25) Wang, J. Q.; Mao, W. W.; Lock, L. L.; Tang, J. B.; Sui, M. H.; Sun, W. L.; Cui, H. G.; Xu, D.; Shen, Y. Q. The Role of Micelle Size in Tumor Accumulation, Penetration, and Treatment. *ACS Nano* **2015**, *9*, 7195−7206.
(26) Cabral, H.; Matsumoto, Y.; Mizuno, K.; Chen, Q.; Murakami, M.; Kimura, M.; Terada, Y.; Kano, M. R.; Miyazono, K.; Uesaka, M.; Nishiyama, N.; Kataoka, K. Accumulation of Sub-100 nm Polymeric Micelles in Poorly Permeable Tumours Depends on Size. *Nat. Nanotechnol.* **2011**, *6*, 815−823.
(27) Tang, L.; Yang, X.; Yin, Q.; Cai, K.; Wang, H.; Chaudhury, I.; Yao, C.; Zhou, Q.; Kwon, M.; Hartman, J. A.; Dobrucki, I. T.; Dobrucki, L. W.; Borst, L. B.; Lezmi, S.; Helferich, W. G.; Ferguson, A. L.; Fan, T. M.; Cheng, J. Investigating the Optimal Size of Anticancer Nanomedicine. *Proc. Natl. Acad. Sci. U. S. A.* **2014**, *111*, 15344−15349.
(28) Huo, S. D.; Ma, H. L.; Huang, K. Y.; Liu, J.; Wei, T.; Jin, S. B.; Zhang, J. C.; He, S. T.; Liang, X. J. Superior Penetration and Retention Behavior of 50 nm Gold Nanoparticles in Tumors. *Cancer Res.* **2013**, *73*, 319−330.
(29) Kirtane, A. R.; Kalscheuer, S. M.; Panyam, J. Exploiting Nanotechnology to Overcome Tumor Drug Resistance: Challenges and Opportunities. *Adv. Drug Delivery Rev.* **2013**, *65*, 1731−1747.
(30) Cheng, R.; Meng, F. H.; Deng, C.; Zhong, Z. Y. Bioresponsive Polymeric Nanotherapeutics for Targeted Cancer Chemotherapy. *Nano Today* **2015**, *10*, 656−670.
(31) Romberg, B.; Hennink, W. E.; Storm, G. Sheddable Coatings for Long-Circulating Nanoparticles. *Pharm. Res.* **2008**, *25*, 55−71.
(32) Sun, H.; Guo, B.; Cheng, R.; Meng, F.; Liu, H.; Zhong, Z. Biodegradable Micelles with Sheddable Poly(Ethylene Glycol) Shells for Triggered Intracellular Release of Doxorubicin. *Biomaterials* **2009**, *30*, 6358−66.
(33) Yang, X. Z.; Du, J. Z.; Dou, S.; Mao, C. Q.; Long, H. Y.; Wang, J. Sheddable Ternary Nanoparticles for Tumor Acidity-Targeted siRNA Delivery. *ACS Nano* **2012**, *6*, 771−781.
(34) Zhu, Y. Q.; Zhang, J.; Meng, F. H.; Deng, C.; Cheng, R.; Feijen, J.; Zhong, Z. Y. cRGD-Functionalized Reduction-Sensitive Shell-Sheddable Biodegradable Micelles Mediate Enhanced Doxorubicin Delivery to Human Glioma Xenografts in Vivo. *J. Controlled Release* **2016**, *233*, 29−38.
(35) Huang, P. S.; Liu, J. J.; Wang, W. W.; Zhang, Y. M.; Zhao, F. L.; Kong, D. L.; Liu, J. F.; Dong, A. J. Zwitterionic Nanoparticles Constructed from Bioreducible Raft-Rop Double Head Agent for Shell Shedding Triggered Intracellular Drug Delivery. *Acta Biomater.* **2016**, *40*, 263−272.
(36) Zhao, C. Y.; Shao, L. H.; Lu, J. Q.; Deng, X. W.; Wu, Y. Tumor Acidity-Induced Sheddable Polyethylenimine-Poly(Trimethylene Carbonate)/DNA/Polyethylene Glycol-2,3-Dimethylmaleicanhydride Ternary Complex for Efficient and Safe Gene Delivery. *ACS Appl. Mater. Interfaces* **2016**, *8*, 6400−6410.
(37) Rao, N. V.; Yoon, H. Y.; Han, H. S.; Ko, H.; Son, S.; Lee, M.; Lee, H.; Jo, D.-G.; Kang, Y. M.; Park, J. H. Recent Developments in Hyaluronic Acid-Based Nanomedicine for Targeted Cancer Treatment. *Expert Opin. Drug Delivery* **2016**, *13*, 239−252.
(38) Oh, E. J.; Park, K.; Kim, K. S.; Kim, J.; Yang, J.-A.; Kong, J.-H.; Lee, M. Y.; Hoffman, A. S.; Hahn, S. K. Target Specific and Long-Acting Delivery of Protein, Peptide, and Nucleotide Therapeutics Using Hyaluronic Acid Derivatives. *J. Controlled Release* **2010**, *141*, 2−12.
(39) Wang, H.; Agarwal, P.; Zhao, S. T.; Yu, J. H.; Lu, X. B.; He, X. M. A near-Infrared Laser- Activated "Nanobomb" for Breaking the Barriers to microRNA Delivery. *Adv. Mater.* **2016**, *28*, 347−355.
(40) Wang, S. P.; Zhang, J. M.; Wang, Y. T.; Chen, M. W. Hyaluronic Acid-Coated PEI-PLGA Nanoparticles Mediated Co-Delivery of Doxorubicin and miR-542−3p for Triple Negative Breast Cancer Therapy. *Nanomedicine* **2016**, *12*, 411−420.
(41) Ravar, F.; Saadat, E.; Gholami, M.; Dehghankelishadi, P.; Mahdavi, M.; Azami, S.; Dorkoosh, F. A. Hyaluronic Acid-Coated Liposomes for Targeted Delivery of Paclitaxel, in-Vitro Characterization and in-Vivo Evaluation. *J. Controlled Release* **2016**, *229*, 10−22.
(42) Martens, T. F.; Remaut, K.; Deschout, H.; Engbersen, J. F. J.; Hennink, W. E.; van Steenbergen, M. J.; Demeester, J.; De Smedt, S. C.; Braeckmans, K. Coating Nanocarriers with Hyaluronic Acid Facilitates Intravitreal Drug Delivery for Retinal Gene Therapy. *J. Controlled Release* **2015**, *202*, 83−92.
(43) Zhang, Q.; Deng, C. F.; Fu, Y.; Sun, X.; Gong, T.; Zhang, Z. R. Repeated Administration of Hyaluronic Acid Coated Liposomes with Improved Pharmacokinetics and Reduced Immune Response. *Mol. Pharmaceutics* **2016**, *13*, 1800−1808.
(44) Zhu, H.; Chen, H.; Zeng, X.; Wang, Z.; Zhang, X.; Wu, Y.; Gao, Y.; Zhang, J.; Liu, K.; Liu, R.; Cai, L.; Mei, L.; Feng, S.-S. Co-Delivery of Chemotherapeutic Drugs with Vitamin E TPGS by Porous PLGA Nanoparticles for Enhanced Chemotherapy against Multi-Drug Resistance. *Biomaterials* **2014**, *35*, 2391−2400.
(45) Chen, J.; Zou, Y.; Deng, C.; Meng, F.; Zhang, J.; Zhong, Z. Multifunctional Click Hyaluronic Acid Nanogels for Targeted Protein Delivery and Effective Cancer Treatment in Vivo. *Chem. Mater.* **2016**, *28*, 8792−8799.

DOI: 10.1021/acsami.6b15105
ACS Appl. Mater. Interfaces 2017, 9, 3985−3994

(46) Zou, Y.; Meng, F.; Deng, C.; Zhong, Z. Robust, Tumor-Homing and Redox-Sensitive Polymersomal Doxorubicin: A Superior Alternative to Doxil and Caelyx? *J. Controlled Release* **2016**, *239*, 149−158.
(47) Knoop, R. J. I.; Habraken, G. J. M.; Gogibus, N.; Steig, S.; Menzel, H.; Koning, C. E.; Heise, A. Synthesis of Poly(Benzyl Glutamate-b-Styrene) Rod-Coil Block Copolymers by Dual Initiation in One Pot. *J. Polym. Sci., Part A: Polym. Chem.* **2008**, *46*, 3068−3077.
(48) Talelli, M.; Barz, M.; Rijcken, C. J. F.; Kiessling, F.; Hennink, W. E.; Lammers, T. Core-Crosslinked Polymeric Micelles: Principles, Preparation, Biomedical Applications and Clinical Translation. *Nano Today* **2015**, *10*, 93−117.
(49) Sun, B.; Deng, C.; Meng, F.; Zhang, J.; Zhong, Z. Robust, Active Tumor-Targeting and Fast Bioresponsive Anticancer Nanotherapeutics Based on Natural Endogenous Materials. *Acta Biomater.* **2016**, *45*, 223−233.
(50) Zhong, Y.; Yang, W.; Sun, H.; Cheng, R.; Meng, F.; Deng, C.; Zhong, Z. Ligand-Directed Reduction-Sensitive Shell-Sheddable Biodegradable Micelles Actively Deliver Doxorubicin into the Nuclei of Target Cancer Cells. *Biomacromolecules* **2013**, *14*, 3723−3730.
(51) Ji, R.; Cheng, J.; Yang, T.; Song, C.-C.; Li, L.; Du, F.-S.; Li, Z.-C. Shell-Sheddable, pH-Sensitive Supramolecular Nanoparticles Based on Ortho Ester-Modified Cyclodextrin and Adamantyl Peg. *Biomacromolecules* **2014**, *15*, 3531−3539.
(52) Zhong, Y. N.; Zhang, J.; Cheng, R.; Deng, C.; Meng, F. H.; Xie, F.; Zhong, Z. Y. Reversibly Crosslinked Hyaluronic Acid Nanoparticles for Active Targeting and Intelligent Delivery of Doxorubicin to Drug Resistant CD44+ Human Breast Tumor Xenografts. *J. Controlled Release* **2015**, *205*, 144−154.
(53) Jeannot, V.; Mazzaferro, S.; Lavaud, J.; Vanwonterghem, L.; Henry, M.; Arboléas, M.; Vollaire, J.; Josserand, V.; Coll, J.-L.; Lecommandoux, S.; Schatz, C.; Hurbin, A. Targeting CD44 Receptor-Positive Lung Tumors Using Polysaccharide-Based Nanocarriers: Influence of Nanoparticle Size and Administration Route. *Nanomedicine* **2016**, *12*, 921−932.
(54) Yang, C.; Wang, X.; Yao, X.; Zhang, Y.; Wu, W.; Jiang, X. Hyaluronic Acid Nanogels with Enzyme-Sensitive Cross-Linking Group for Drug Delivery. *J. Controlled Release* **2015**, *205*, 206−217.
(55) Yang, J.-A.; Kong, W. H.; Sung, D. K.; Kim, H.; Kim, T. H.; Lee, K. C.; Hahn, S. K. Hyaluronic Acid-Tumor Necrosis Factor-Related Apoptosis-Inducing Ligand Conjugate for Targeted Treatment of Liver Fibrosis. *Acta Biomater.* **2015**, *12*, 174−182.
(56) Zhong, Y.; Goltsche, K.; Cheng, L.; Xie, F.; Meng, F.; Deng, C.; Zhong, Z.; Haag, R. Hyaluronic Acid-Shelled Acid-Activatable Paclitaxel Prodrug Micelles Effectively Target and Treat CD44-Overexpressing Human Breast Tumor Xenografts in Vivo. *Biomaterials* **2016**, *84*, 250−261.
(57) Li, S.; Zhang, J.; Deng, C.; Meng, F. H.; Yu, L.; Zhong, Z. Y. Redox-Sensitive and Intrinsically Fluorescent Photoclick Hyaluronic Acid Nanogels for Traceable and Targeted Delivery of Cytochrome C to Breast Tumor in Mice. *ACS Appl. Mater. Interfaces* **2016**, *8*, 21155−21162.
(58) Tengdelius, M.; Gurav, D.; Konradsson, P.; Pahlsson, P.; Griffith, M.; Oommen, O. P. Synthesis and Anticancer Properties of Fucoidan-Mimetic Glycopolymer Coated Gold Nanoparticles. *Chem. Commun.* **2015**, *51*, 8532−8535.
(59) Wang, H.; Agarwal, P.; Zhao, S. T.; Xu, R. X.; Yu, J. H.; Lu, X. B.; He, X. M. Hyaluronic Acid-Decorated Dual Responsive Nanoparticles of Pluronic F127, PLGA, and Chitosan for Targeted Co-Delivery of Doxorubicin and Irinotecan to Eliminate Cancer Stem-Like Cells. *Biomaterials* **2015**, *72*, 74−89.
(60) Du, J. B.; Cheng, Y.; Teng, Z. H.; Huan, M. L.; Liu, M.; Cui, H.; Zhang, B. L.; Zhou, S. Y. pH-Triggered Surface Charge Reversed Nanoparticle with Active Targeting to Enhance the Antitumor Activity of Doxorubicin. *Mol. Pharmaceutics* **2016**, *13*, 1711−1722.
(61) Duhem, N.; Danhier, F.; Preat, V. Vitamin E-Based Nanomedicines for Anti-Cancer Drug Delivery. *J. Controlled Release* **2014**, *182*, 33−44.
(62) Youk, H.-J.; Lee, E.; Choi, M.-K.; Lee, Y.-J.; Chung, J. H.; Kim, S.-H.; Lee, C.-H.; Lim, S.-J. Enhanced Anticancer Efficacy of α-Tocopheryl Succinate by Conjugation with Polyethylene Glycol. *J. Controlled Release* **2005**, *107*, 43−52.
(63) Hu, Q. Z.; Rijcken, C. J.; Bansal, R.; Hennink, W. E.; Storm, G.; Prakash, J. Complete Regression of Breast Tumour with a Single Dose of Docetaxel-Entrapped Core-Cross-Linked Polymeric Micelles. *Biomaterials* **2015**, *53*, 370−378.
(64) Liang, M. M.; Fan, K. L.; Zhou, M.; Duan, D. M.; Zheng, J. Y.; Yang, D. L.; Feng, J.; Yan, X. Y. H-Ferritin-Nanocaged Doxorubicin Nanoparticles Specifically Target and Kill Tumors with a Single-Dose Injection. *Proc. Natl. Acad. Sci. U. S. A.* **2014**, *111*, 14900−14905.

DOI: 10.1021/acsami.6b15105
ACS Appl. Mater. Interfaces 2017, 9, 3985−3994